

## The potential of imaging subsurface heterogeneities by natural local earthquakes

Yohei Nishitsuji<sup>1</sup>, Issei Doi<sup>2</sup>, and Deyan Draganov<sup>3</sup>

### ABSTRACT

We have developed a new imaging technique of subsurface heterogeneities that uses Sp-waves from natural earthquakes. This technique can be used as a first screening tool in frontier exploration areas before conventional active exploration. Analyzing Sp-waves from 28 earthquakes ( $M_j$  2.0 to 4.2) recorded by two permanent seismic stations, we built an image of the distributions of velocity discontinuities in southeastern offshore Hokkaido, Japan, where intraplate earthquakes in the Pacific plate frequently occur. Our results indicated the presence of three horizontally continuous, distinct discontinuities corresponding to geologic boundaries estimated in a previous study. We also derived the frequency-dependent quality factor  $Q$  for P- and S-waves and use it as a method of characterizing physical properties of subsurface structure. The waveform traces with coherent Sp-phases in the southern part of the study area generally show a constant  $Q_S/Q_P$  ratio, and the waveform traces with randomly distributed phases in the northern part show a large variation of the  $Q_S/Q_P$  ratio (including several high values).

### INTRODUCTION

Imaging heterogeneities in the subsurface is a crucial topic in hydrocarbon exploration as well as academia. However, acquiring these images using conventional active sources (e.g., explosives, vibroseis, and airgun) is not always easily achievable because of costs, environmental concerns, and other practical issues. Therefore, the use of passive seismic methods, such as microseism

reflection imaging (e.g., Toksöz, 1964; Tamakawa et al., 2010; Reshetnikov et al., 2012) and seismic interferometry with ambient noise (e.g., Draganov et al., 2009; Ruigrok et al., 2011, 2012; Grechka and Zhao, 2012), has recently become more attractive. In this sense, despite the fact that earthquakes are usually seen as abhorrent phenomena in human communities (due to the risks they pose), it is natural to also view weaker earthquakes as attractive natural resources if one can use their information in appropriate analyses. In this study, we propose a new passive imaging technique with spatial resolution higher than the one normally achieved with already established passive seismic techniques using naturally occurring earthquakes. Our technique could be used as a first screening tool for frontier exploration areas with limited available seismic surveys and before a decision is made for acquisition with conventional surveys with active sources.

There are several methods for using earthquakes to image velocity discontinuities in the subsurface, such as reflection (e.g., James and Savage, 1990) and receiver-function (e.g., Langston, 1979) analyses. However, reflection analysis can image only the parts of the subsurface deeper than the focal depths. The receiver-function method uses waves coming from the deeper part to the surface, which enables one to obtain information of the shallower subsurface structure. This method, however, uses teleseismic events with large magnitudes. As a result, high spatial resolution may not be expected from this method because the expected frequencies at the receivers would be relatively lower than the frequencies recorded from local earthquakes. Because of this, it is important to have a method to image the shallower parts of the subsurface with higher spatial resolution in areas where natural resources (e.g., hydrocarbons) are found and produced.

Doi and Kawakata (2013) propose a new method to image subsurface velocity discontinuities with relatively higher resolution using a different type of seismic phase — Sp-waves. Advantages

Nishitsuji, Y. and Doi, I. (2012) A method to estimate seismic heterogeneity through Sp-waves and frequency dependent quality factor  $Q$  analyses: A case study in southeastern offshore of Hokkaido, Japan: SEG Technical Program Expanded Abstracts 2012, doi: <http://dx.doi.org/10.1190/segam2012-0630.1>. Manuscript received by the Editor 23 October 2013; revised manuscript received 19 July 2014; published online 23 October 2014.

<sup>1</sup>Presently Delft University of Technology, Department of Geosciences and Engineering, Delft, the Netherlands; formerly Mitsui Oil Exploration Co., Ltd., Exploration & Production Division, Tokyo, Japan. E-mail: y.nishitsuji@tudelft.nl.

<sup>2</sup>Kyoto University, Disaster Prevention Research Institute, Kyoto, Japan. E-mail: doi.issei.5e@kyoto-u.ac.jp.

<sup>3</sup>Delft University of Technology, Department of Geosciences and Engineering, Delft, the Netherlands. E-mail: d.s.draganov@tudelft.nl.

© 2014 Society of Exploration Geophysicists. All rights reserved.

of this method are that one could avoid having to treat the possible strong amplitudes of the S-waves and that one expects to have higher resolution because local, weaker earthquakes can be used (which thus have signals with higher frequency content).

However, having only an image of the discontinuities might not be sufficient to estimate the physical properties of the subsurface structures because the amplitudes of the converted or reflected waves depend on the densities as well as P- and S-wave velocities below and above the discontinuities. The quality factor  $Q$ , characteristic of the attenuation, could provide one with additional information to estimate the condition of the medium. For seismic exploration, [Klimentov \(1995\)](#) suggests that the  $Q_S/Q_P$  ratio estimated from well-log data could be used as a tool for distinguishing gas and condensate from oil and water, and [Zarean et al. \(2008\)](#) report that a high value of the  $Q_S/Q_P$  ratio, obtained from the spectra of earthquake coda, could be related to strong heterogeneity, such as a highly fractured area.

Thus, integrated analysis of Sp-waves and the  $Q_S/Q_P$  ratio could be a useful tool to characterize heterogeneous structures in the shallower part of the crust. In the following, we show how to apply such analysis to field waveform data.

## DATA SET AND STUDY AREA

We analyzed 40 waveforms from 28 earthquakes, which occurred from 28 September 2002 to 4 April 2011 offshore, southeast of

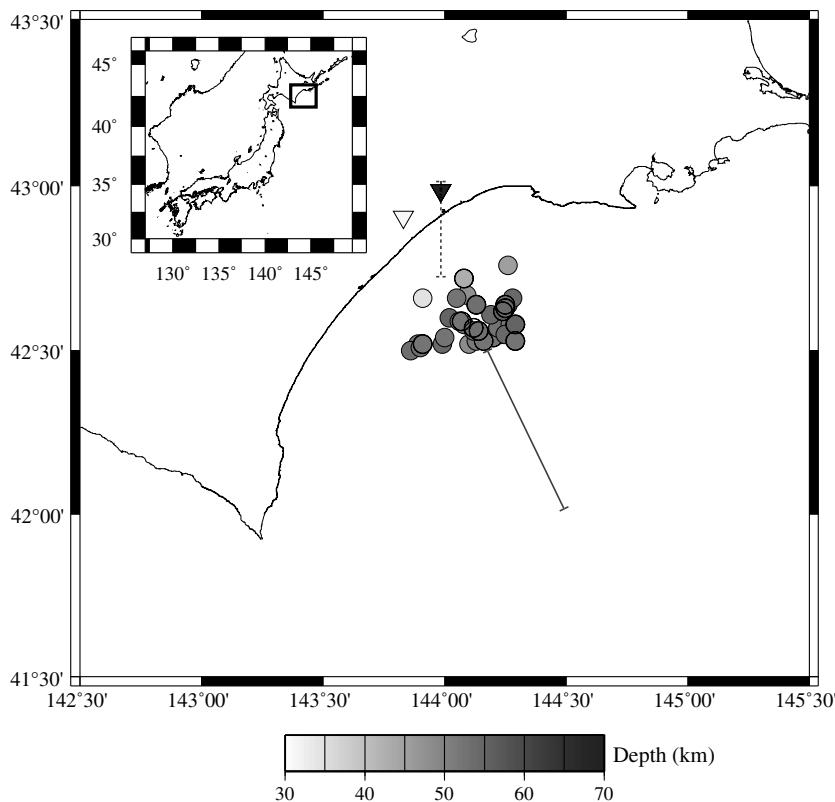


Figure 1. Map of the study area showing the position of the two stations (N.SNSH, black triangle; ONBETS, white triangle) and the hypocenter distribution of the 28 earthquakes (circles) used in this work provided by NIED and JMA. The grayscale of the circles indicates the event depth. The dashed and solid lines indicate the profile lines where the seismic images are obtained in this study and in [Honza \(1999\)](#), respectively.

Hokkaido, Japan. The earthquakes were recorded by two nearby seismic stations: ONBETS, operated by the Japan Meteorological Agency (JMA), and N.SNSH, operated by the National Research Institute for Earth Science and Disaster (NIED). The locations of the epicenters and the seismic stations are shown in Figure 1. The magnitudes of the earthquakes we used were in the range of  $M_j$  (the local magnitude defined and calculated by JMA) 2.0 to 4.2. We excluded larger events from our analysis because these may have a relatively longer source-time duration, which would cause difficulties in imaging with Sp-waves and in the spectral analysis.

We have access to an active-source seismic profile (see the black solid line in Figure 1), which was shot close to our study area ([Honza, 1999](#)). The seismic section (GH76-2) was acquired in 1976 by the Geological Survey of Japan (currently the National Institute of Advanced Industrial Science and Technology) under a contract from Japan's Ministry of International Trade and Industry (currently Japan's Ministry of Economy, Trade, and Industry).

## Sp-WAVE ANALYSIS

### Method

Following the pioneering work of [Doi and Kawakata \(2013\)](#), we briefly show what Sp-waves are and how they could be analyzed. An S-wave incident with an angle on a velocity discontinuity from a

source (in our case, a local earthquake) splits in its upward propagation into P- and S-waves. The converted P-waves (Sp-waves) arrive at the station earlier than the direct S-waves (Figure 2). The Sp-waves have lower amplitudes than do the direct S-waves. Figure 3 shows the vertical and transverse components of the recorded displacement waveforms for events with depths between 50 and 60 km after application of a band-pass filter between 2 and 5 Hz. The vertical locations of the traces are proportional to the P-wave traveltimes. To estimate the slownesses of the phases needed here, one would normally plot the waveforms in terms of epicentral distances. However, we use the P-wave traveltimes, which are approximately proportional to the hypocentral distance, because the focal depths of the earthquakes are different. The horizontal axis is reduced such that the S-phases are aligned almost vertically. The Sp-waves may contain frequencies higher than 5 Hz. Still, the range of our band-pass filtering was chosen so that any influence from local scattering is suppressed. A similar result could be obtained by using frequencies lower than 2 Hz; however, in our case, such a filter does not result in a better identification. To minimize the effect of P-wave coda during the use of the Sp-waves, we use the time window starting 3.5 s after the onset of the P-waves and finishing at the onset of the S-waves.

In Figure 3, we observe three coherent Sp-phases as indicated by the dashed-dotted and dotted lines. To confirm that those phases are indeed Sp-phases, we analyze their particle motion.

Figure 4 shows three particle-motion plots, which are sampled from the vertical- and transverse-component waveforms highlighted with bold black in Figure 3. The three time windows correspond to the times indicated in Figure 3 as possibly containing Sp-phases. The particle-motion plots reveal what is also expected as a typical feature of the Sp-waves — predominant vertical motion because the recorded waves are converted P-waves.

For seismograms with different epicentral distances and focal depths, Sp-waves arrive with a different time separation relative to the S-wave arrival, even if generated by the same horizontal velocity discontinuity. Assuming a half-layer subsurface model, the recorded direct S- and Sp-waves at the same receiver from the same source will be characterized by different angles due to the Sp-waves' conversion at depth  $h$  (see Figure 2). The traveltime difference between the Sp-waves and the direct S-waves  $\Delta t$  is a function of the conversion depth  $h$ . Thus,  $h$  can be obtained from the estimated  $\Delta t$  (Doi and Kawakata, 2013), given a certain velocity model. The Sp-phases will align along the conversion-depth axis if they are generated by the same horizontal velocity discontinuity. P-wave coda or Sp-reverberations will not align because we use earthquakes with varying epicentral distances and focal depths.

We calculate  $h$  by trial and error using ray tracing. In this study, we use a simple homogeneous background velocity model ( $V_P = 6.4$  km/s and  $V_S = 3.7$  km/s) taken from Miyamachi et al.

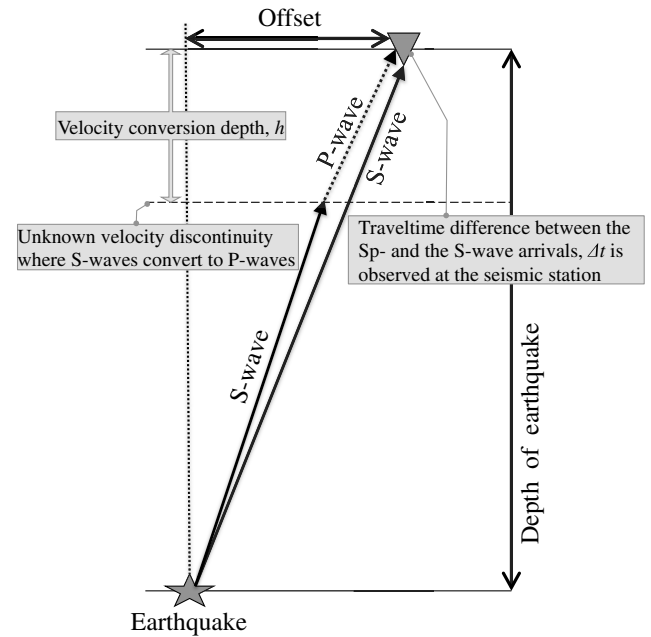


Figure 2. Sp- and S-wave are recorded at the seismic station. The vertical and horizontal distances are 25 and 60 km, respectively, which is in the same scale as the geometry in this study.

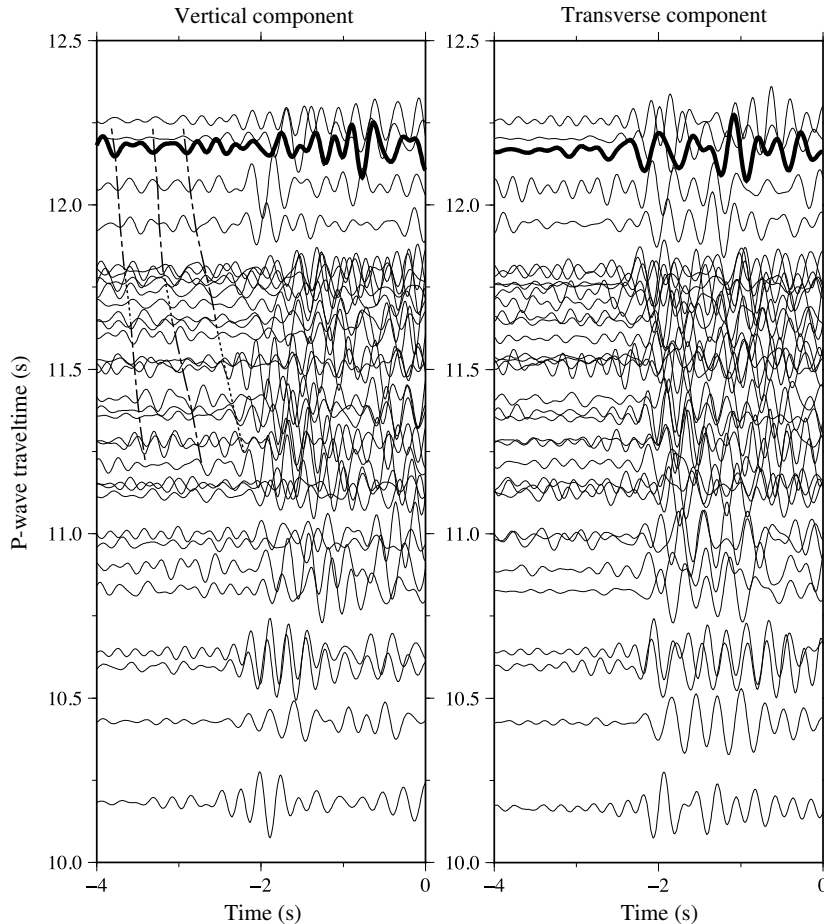


Figure 3. Sorted seismograms (depth between 50 and 60 km) from the vertical and transverse components as a function of the traveltimes of the P-wave. The horizontal axis is reduced such that the S-waves align vertically. The trace highlighted in bold indicates the example waveform for the particle-motion analysis shown in Figure 4. The dashed-dotted and dashed lines indicate the Sp-wave candidates with and without clear visual coherency among neighboring traces, respectively.

(1994) who estimate the crustal velocity structure in northern Japan using traveltimes tomography. When desired, one could consider a depth-dependent velocity structure. However, calculation using several possible models showed that the expected bending had a smaller effect on the results compared with the spatial resolution (2.5 km in the horizontal direction) expected in our study.

Wilson et al. (2006) report that there is a constraint for the receiver function to use Sp-waves because other teleseismic phases (e.g., pPPP and SKSp) arrive simultaneously with the Sp-phases. Because we use local earthquakes, the expected Sp-waves on the records must be completely free of the mentioned contaminating phases.

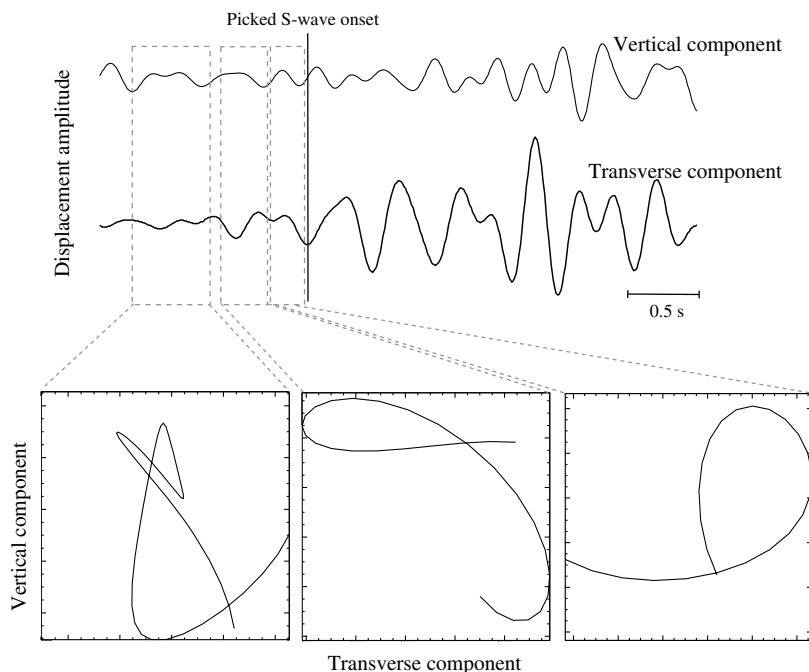


Figure 4. Examples of the particle motions. The three time windows are taken around the Sp-phase arrival times as indicated in Figure 3. The scale of the vertical axes is the same in the two upper panels (seismograms); the scales of the horizontal and vertical axes of the particle motions are also the same. The seismogram was recorded by N.SNSH with the origin time at 00:22:42 on 3 October 2003.

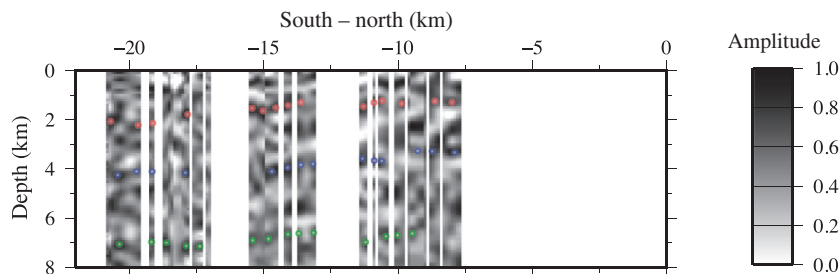


Figure 5. Averaged amplitude of envelopes for Sp-waves as a function of the horizontal distance from N.SNSH for points at a conversion depth of 4 km. The northern origin location at  $43.0^\circ$  in latitude and  $144.0^\circ$  in longitude is set as 0 km in the horizontal axis. Red, blue, and green dots represent phases of large amplitudes with lateral coherency.

## Results

In Figure 5, we show the averaged amplitude of the envelopes, which are calculated for waveform traces whose conversion points at the same depths for Sp-waves are very close to each other. The averaged amplitudes are ordered as a function of the distance from N.SNSH to the positions of the conversion points at a depth of 4 km. Thus, the averaged amplitudes given at another depth only indicate a model with a possible conversion point at that depth, but not the exact horizontal location of the trace. The blank (gap) areas in Figure 5 represent areas where the available earthquakes cannot cause a conversion at a depth of 4 km. In Figure 5, we have indicated three laterally coherent phases, highlighted by red (1.0 to 2.5 km), blue (3.0 to 4.5 km), and green (6.5 to 7.0 km) dots. Because these phases are coherent and dominant in the vertical component (see Figure 4), we interpret these phases as resulting from the presence of velocity discontinuities that cause S-to-P conversions at those depths.

To check and possibly confirm the interpretation from Figure 5, and also to understand the distributions of the velocity discontinuities in three dimensions, we spatially stack the amplitudes of the envelopes of the Sp-waves. The stacking procedure is as follows: The origin of the offset is set at  $43.0^\circ$  in latitude and  $144.0^\circ$  in longitude, which is near station N.SNSH. We set a projection plane together with the  $x$ - and  $y$ -axes, which are parallel and perpendicular to it, respectively. We discretize the 3D model to consist of bins defined by 2.5 ( $x$ -offset), 2.5 ( $y$ -offset), and 0.5 km (depth). The conversion points are computed by ray tracing for every possible Sp-wave arriving at the stations with 0.01 s intervals. The amplitudes of the waveforms that fall in the same bin are summed. Finally, we average the summed amplitudes by the number of the traces that fall in that bin.

The summed amplitudes along the north-south cross section with a back azimuth of  $350^\circ$  are shown in Figure 6. In the cross section, we can see parts with relatively strong continuous amplitudes at depths of 1.0–2.0 km (shown with red arrows), 3.0–4.5 km (shown with blue arrows), and 7.0–7.5 km (shown with green arrows) in the southern section. Although it is not as distinct, we also detect two continuous amplitudes in the northern section (shown with dotted arrows). Note that the three coherent phases in Figure 5 mainly contribute to the blocks with large amplitudes in Figure 6. For example, the strong-amplitude blocks between  $-22.5$  and  $-15$  km lateral direction and at a depth of around 7.0 km in Figure 6 are attributed to the phases with green dots in Figure 5.

The image in Figure 6 gives us confidence in our interpretation in Figure 5 because randomly distributed phases with high amplitudes would not provide any similarity between our interpretations (Figure 5) and the amplitude continuity (Figure 6).

The spatial distribution of the velocity discontinuities along two more cross sections is shown in Figure 7. The stacked images are projected from the northern origin point described above to 22.5 km south with back azimuth of 340° and 360°. Because of the spatial distribution of the earthquakes and the position of the stations, as well as the spatial resolution (bin size), the imaging nearby the northern origin point shows a similar or identical result along the different projection planes. The interpreted features along the projection plane with the 350° azimuth (Figure 6 and the green frame in Figure 7) are continuous (and can be interpreted) in the eastern and western directions.

## FREQUENCY-DEPENDENT $Q$

### Method

We estimate  $Q$  for P- and S-waves using a frequency-dependent model to investigate a possible relationship with the detected velocity discontinuities by Sp-waves. [Abercrombie \(1995\)](#) estimates corner frequency and  $Q$  by using a single corner frequency source model of the far-field displacement spectrum with frequency-independent  $Q$ . We modify the author's method, assuming  $Q$  to be proportional to frequency to the power of a constant. With a reference to the standard source model of [Brune \(1970, 1971\)](#), which assumes a point-source model keeping constant radiated energy ratio between P- and S-waves for different sizes of magnitudes, the corner frequency of the far-field term is derived based on the so-called  $\omega_{-2}$ -model from [Aki \(1967\)](#). We extract a window of 3-s length around each identified P- and S-wave arrival from the recorded seismic waveforms. The windows are transformed to the temporal frequency domain using a fast Fourier transform with a 10% taper. We estimate  $Q_P$  and  $Q_S$  as a function of frequency and the corner frequency with a grid-search method, so as to fit the observed P- and S-wave spectrum in the frequency band of 1–20 Hz. We use this frequency band because it has high signal-to-noise ratios. An example of the fitting for the  $Q_P$ - and  $Q_S$ -values is shown in Figure 8. Subsequently, we calculate the value of the  $Q_S/Q_P$  ratio for every waveform trace recorded at the station. The effect of focal mechanisms is not considered because we did not estimate the seismic moment in this study.

### Results

In Figure 9, we show the estimated values of the  $Q_S/Q_P$  ratio at 3.5 Hz, which is inside the range of the band-pass filter we apply for the use of Sp-waves. Each dot represents the  $Q_S/Q_P$  ratio of each trace, which passes through the shown lateral distance for the conversion depth of 4 km. For the northern part (lateral distance between –7.5 and –11 km), we see that the  $Q_S/Q_P$  ratios show large variations including

several values higher than 1.5. In contrast, the  $Q_S/Q_P$  ratios exhibit less scatter in the southern part.

## DISCUSSION

[Honza \(1999\)](#) presents results from subsurface imaging obtained using conventional active sources (airguns) along a seismic line a few tens of kilometers away toward the southeast direction from the area of our study. The author interpreted three major geologic horizons: top Quaternary, top Pliocene, and top of lower Miocene. These geologic horizons are interpreted in [Honza \(1999\)](#) as slightly inclined in the north-northwest direction. The depths and trends of these three horizons correspond to the velocity discontinuities found in our study (e.g., Figure 6).

[Aki \(1992\)](#) argues that the scattering waves with conversions from P- to S-waves would be more commonly generated than the scattering with conversion from S- to P-waves. This could be interpreted as the P-waves being attenuated more than the S-waves. In our study, coherent Sp-waves are mainly found in the southern part

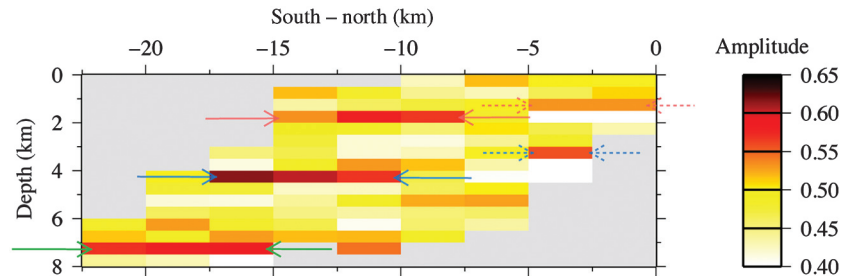


Figure 6. Stacked seismic section of the Sp-waves envelopes. The color indicates the stacked amplitude. The horizontal axis is identical to the one in Figure 5. The solid and dashed arrows indicate locations where relatively strong and moderate amplitudes (higher than 0.5), respectively, are interpreted as laterally continuous features.

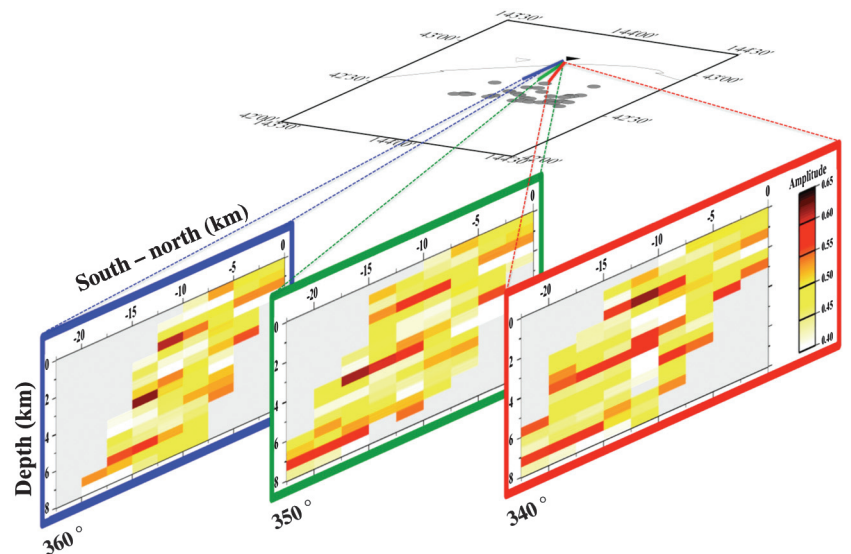


Figure 7. Stacked sections, as the one in Figure 6, shown as a function of back azimuth. The green-framed section in the middle corresponds to the section of Figure 6. The red- and blue-framed sections have 10° back-azimuth differences with respect to the middle stacked section.

in Figure 6, for which we can observe in Figure 9 a relatively smaller variation of the  $Q_S/Q_P$  ratios. On the other hand, we could detect less coherent phases in the northern part, for which we observe the relatively larger variation of the  $Q_S/Q_P$  ratios (with several high values of  $>1.5$ ). It is possible that the geologic layers of the Quaternary, Pliocene, and Miocene periods generate the coherent converted waves in the southern part, whereas strong heterogeneity disturbs the wavefield in the northern part.

Using well-log data, Klimentos (1995) demonstrates that a high value of the  $Q_S/Q_P$  ratio would indicate the presence of gas, and Zarean et al. (2008) report that a high value of the  $Q_S/Q_P$  ratio, obtained using records of natural earthquakes, could be related to highly fractured areas. This means that a possible interpretation of our result for the northern part of the study area, which exhibits relatively higher  $Q_S/Q_P$  ratios, may be attributed to well-developed fractures and/or the presence of gas.

Integrating the information of converted-wave amplitudes and relative  $Q_S/Q_P$  ratios can be used to interpret the physical properties of certain layers. However, the resolution of the images is dependent on how densely the raypaths are distributed in the area of interest; in other words, it fully relies on the positions of the earthquakes (passive sources) and receivers. For example, the  $Q$ -values estimated here are interpreted as representative for the complete raypaths. When more earthquakes or stations are available, identifying the depth of most attenuated locations could be done with a higher spatial resolution due to the available variety of crossing raypaths.

Another possibility is to try to use the method proposed recently by Draganov et al. (2010, 2013) for estimation of a layer-specific  $Q$ -value. In this method, the authors propose to use nonphysical (ghost) arrivals retrieved from seismic interferometry applied to records at the surface from subsurface sources. The ghost arrivals are

retrieved from crosscorrelation (or autocorrelation) and summation of specific arrivals from the subsurface sources and represent reflected energy that would have been measured from the bottom of a specific layer as if with a source and receiver placed directly on top of that layer. The retrieval of such ghost arrivals is directly dependent on the  $Q$ -value of the overburden above the layer that causes a ghost. If the method were applied by autocorrelation to each of the two stations from the example we showed, then it would be sufficient to have recordings from earthquakes below the stations. Separate estimation of the  $Q_S$ - and  $Q_P$ -value of the top layer could be done from separate S- and P-wave arrivals, respectively. The application of this method would require P- and S-wave arrivals with near-vertical incidence. This means that we would require other earthquakes than those we used for the interpretation of Sp-wave conversion points. This is so because for a conversion to take place, earthquakes away from the stations were needed. Having more stations would also be helpful to facilitate the overlap between

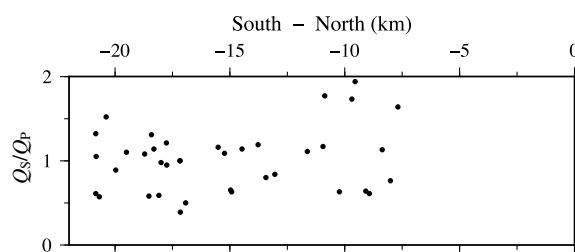


Figure 9. The  $Q_S/Q_P$  ratios as a function of the horizontal distance from N.SNSH. The horizontal axis is identical to those in Figures 5 and 6.

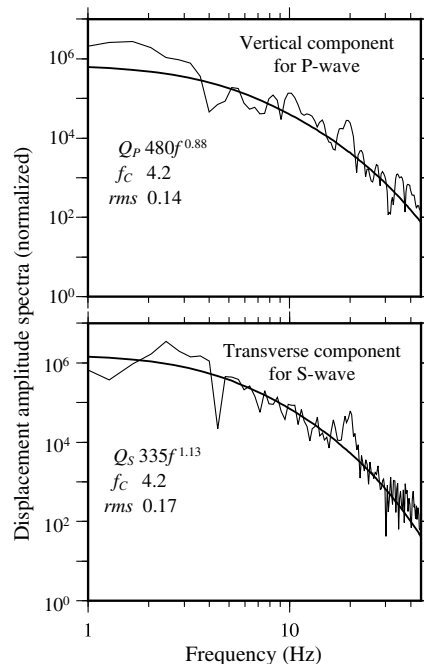
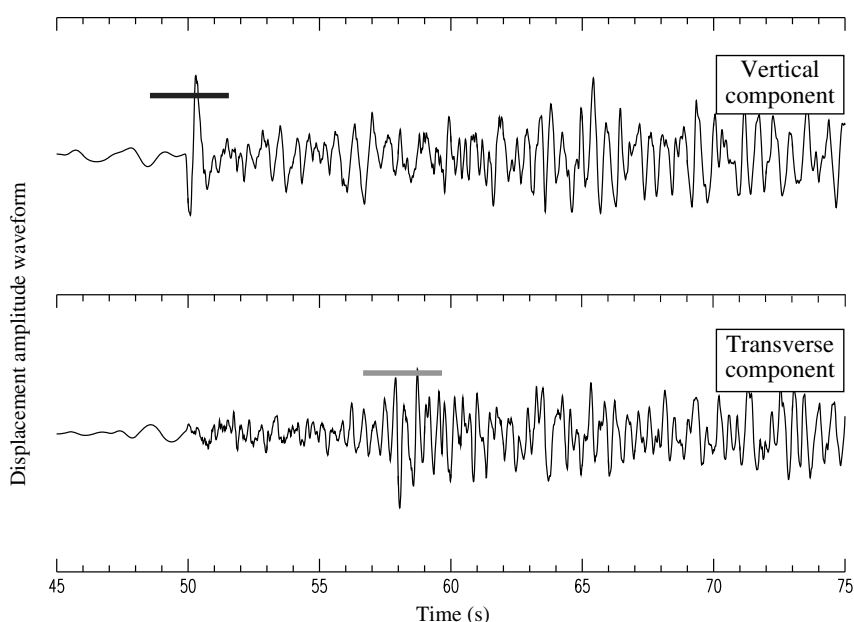


Figure 8. Example of spectral fitting of the data. The seismogram was recorded by N.SNSH with origin time at 01:49:38 on 6 May 2009. The black and gray bars above the vertical and horizontal component of the seismogram indicate the time windows used for  $Q_P$  and  $Q_S$  estimation, respectively. The black curved lines in the spectra show the best-fit results of the grid searching.

the Sp-wave stacked sections and the information about  $Q_S/Q_P$  ratios extracted from ghost reflections.

Further investigation in different locations with hydrocarbons where natural earthquakes occur often (e.g., the west coast of North America, Chile, and Argentina) would help further verify the method we propose.

## CONCLUSION

We presented a method to estimate seismic heterogeneity on the basin scale with Sp-waves and frequency-dependent quality-factor analysis using local earthquakes. We imaged horizontal velocity discontinuities using Sp-waves originating in the southeast of Hokkaido, Japan. Our interpretation is supported by results of an active-source survey carried out nearby. We combined the results of the Sp-waves with results for a distribution of the  $Q_S/Q_P$  ratio below the same area. This allowed us to identify a zone in the south, characterized by a relatively constant  $Q_S/Q_P$  ratio and clearer velocity discontinuities; we also identified a zone in the north, characterized by a relatively larger variation in the  $Q_S/Q_P$  ratio (with several high values) and less clear velocity discontinuities. The latter might be interpreted as a fractured zone, for example. Although it fully relies on the positions of the earthquakes, receivers, and the area of interest, the proposed method could be used as a first screening tool to investigate frontier exploration areas in which limited previous active-source seismic data are available. The regions in which natural earthquakes occur could have favorable conditions to apply the method we presented here.

## ACKNOWLEDGMENTS

The authors thank the National Research Institute for Earth Science and Disaster Prevention and the Japan Meteorological Agency for the data set used in this study. The authors are also grateful to M. Dino Sacchi, the assistant editor, and four anonymous reviewers for their constructive comments that helped to improve the quality of this manuscript. Y. N. is thankful to Mitsui Oil Exploration Co., Ltd. Seismic Analysis Code (SAC2000) was used for a part of the data processing. The maps and graphs were drawn with GenericMappingTool (GMT; Wessel and Smith, 1991).

## REFERENCES

- Abercrombie, R. E., 1995, Earthquake source scaling relationships from  $-1$  to 5 ML using seismograms recorded at 2.5-km depth: *Journal of Geophysical Research*, **100**, 24015–24036, doi: [10.1029/95JB02397](https://doi.org/10.1029/95JB02397).
- Aki, K., 1967, Scaling law of seismic spectrum: *Journal of Geophysical Research*, **72**, 1217–1231, doi: [10.1029/JZ072i004p01217](https://doi.org/10.1029/JZ072i004p01217).
- Aki, K., 1992, Scattering conversions P to S versus S to P: *Bulletin of the Seismological Society of America*, **82**, 1969–1972.
- Brune, J. N., 1970, Tectonic stress and spectra of seismic shear waves from earthquakes: *Journal of Geophysical Research*, **75**, 4997–5009, doi: [10.1029/JB075i026p04997](https://doi.org/10.1029/JB075i026p04997).
- Brune, J. N., 1971, Correction: Tectonic stress and spectra of seismic shear waves from earthquakes: *Journal of Geophysical Research*, **76**, 5002, doi: [10.1029/JB076i020p05002](https://doi.org/10.1029/JB076i020p05002).
- Doi, I., and H. Kawakata, 2013, High resolution spatial distribution of the velocity discontinuities in and around the swarm region beneath the Wakayama district, southwest Japan: *Bulletin of the Seismological Society of America*, **103**, 2135–2141, doi: [10.1785/0120120316](https://doi.org/10.1785/0120120316).
- Draganov, D., X. Campman, J. Thorbecke, A. Verdel, and K. Wapenaar, 2009, Reflection images from ambient seismic noise: *Geophysics*, **74**, no. 5, A63–A67, doi: [10.1190/1.3193529](https://doi.org/10.1190/1.3193529).
- Draganov, D., R. Ghose, K. Heller, and E. Ruigrok, 2013, Monitoring of changes in velocity and  $Q$  using non-physical arrivals in seismic interferometry: *Geophysical Journal International*, **192**, 699–709, doi: [10.1093/gji/ggs037](https://doi.org/10.1093/gji/ggs037).
- Draganov, D., R. Ghose, E. Ruigrok, J. Thorbecke, and K. Wapenaar, 2010, Seismic interferometry, intrinsic losses and  $Q$ -estimation: *Geophysical Prospecting*, **58**, 361–373, doi: [10.1111/j.1365-2478.2009.00828.x](https://doi.org/10.1111/j.1365-2478.2009.00828.x).
- Grechka, V., and Y. Zhao, 2012, Microseismic interferometry: The Leading Edge, **31**, 1478–1483, doi: [10.1190/tle31121478.1](https://doi.org/10.1190/tle31121478.1).
- Honza, E., 1999, Evolution of sedimentary basins in the northern and southern Hokkaido offshore area since the late Miocene: *Chishitsu News*, **542**, 11–22.
- James, D. E., and M. K. Savage, 1990, A search for seismic reflections from the top of the oceanic crust beneath Hawaii: *Bulletin of the Seismological Society of America*, **80**, 675–701.
- Klimentos, T., 1995, Attenuation of P- and S-waves as a method of distinguishing gas and condensate from oil and water: *Geophysics*, **60**, 447–458, doi: [10.1190/1.1443782](https://doi.org/10.1190/1.1443782).
- Langston, C. A., 1979, Structure under Mount Rainier, Washington, inferred from teleseismic body waves: *Journal of Geophysical Research*, **84**, 4749–4762, doi: [10.1029/JB084iB09p04749](https://doi.org/10.1029/JB084iB09p04749).
- Miyamachi, H., M. Kasahara, S. Suzuki, K. Tanaka, and A. Hasegawa, 1994, Seismic velocity structure in the crust and upper mantle beneath northern Japan: *Journal of Physics of the Earth*, **42**, 269–301, doi: [10.4294/jpe1952.42.269](https://doi.org/10.4294/jpe1952.42.269).
- Reshetnikov, A., J. Kummerow, S. A. Shapiro, H. Asanuma, and M. Häring, 2012, Multi-source multi-receiver microseismic reflection imaging: Case study Basel: 82nd Annual International Meeting, SEG, Expanded Abstracts, doi: [10.1190/segam2012-1192.1](https://doi.org/10.1190/segam2012-1192.1).
- Ruigrok, E., X. Campman, and K. Wapenaar, 2011, Extraction of P-wave reflections from microseisms: *Comptes Rendus Geoscience*, **343**, 512–525, doi: [10.1016/j.crte.2011.02.006](https://doi.org/10.1016/j.crte.2011.02.006).
- Ruigrok, E., X. Campman, and K. Wapenaar, 2012, Basin delineation with a 40-hour passive seismic record: *Bulletin of the Seismological Society of America*, **102**, 2165–2176, doi: [10.1785/0120110242](https://doi.org/10.1785/0120110242).
- Tamakawa, K., H. Asanuma, H. Niitsuma, and N. Soma, 2010, Reflection imaging using microseismic multiplets as a source: 80th Annual International Meeting, SEG, Expanded Abstracts, 2166–2170, doi: [10.1190/1.3513274](https://doi.org/10.1190/1.3513274).
- Toksöz, M. N., 1964, Microseisms and an attempted application to exploration: *Geophysics*, **29**, 154–177, doi: [10.1190/1.1439344](https://doi.org/10.1190/1.1439344).
- Wessel, P., and W. H. F. Smith, 1991, Free software helps map and display data: *EOS Transactions AGU*, **72**, 441–448, doi: [10.1029/90EO00319](https://doi.org/10.1029/90EO00319).
- Wilson, D. C., D. A. Angus, J. F. Ni, and S. P. Grand, 2006, Constraints on the interpretation of S-to-P receiver functions: *Geophysical Journal International*, **165**, 969–980, doi: [10.1111/j.1365-246X.2006.02981.x](https://doi.org/10.1111/j.1365-246X.2006.02981.x).
- Zarean, A., M. Farrokhi, and S. Chaychizadeh, 2008, Attenuation of high frequency P and S waves in Qeshm Island, Iran: Presented at 14th World Conference on Earthquake Engineering, IAEE.